Eur. Phys. J. D **31**, 307–311 (2004)
DOI: 10.1140/epjd/e2004-00140-1

THE EUROPEAN PHYSICAL JOURNAL D

Buffer-gas cooling of NH via the beam loaded buffer-gas method

D. Egorov, W.C. Campbell, B. Friedrich[a], S.E. Maxwell, E. Tsikata, L.D. van Buuren, and J.M. Doyle[b]

Department of Physics, Harvard University, Cambridge, MA 02138, USA

Received 20 July 2004
Published online 26 October 2004 –

Abstract. NH radicals from a molecular beam are cooled using a novel beam-loaded buffer gas method. The radicals are produced in a glow discharge beam source and injected into cryogenic helium gas. Up to 10^{12} molecules in their ground electronic, vibrational, and rotational state are detected in the buffer gas and translational temperatures under 6 K are achieved. The cooling method presented is general and can be applied to any molecules in a molecular beam.

PACS. 33.80.Ps Optical cooling of molecules; trapping – 34.50.Ez Rotational and vibrational energy transfer – 39.10.+j Atomic and molecular beam sources and techniques

1 Introduction

There is significant current interest in producing cold and trapped molecules. The ability to cool and trap samples of atoms has led to dramatic advances in atomic physics. Bose-Einstein condensation [1], Fermi degeneracy [2], superfluidity in a dilute atomic gas [3], and atom lasers [4] all became possible once techniques to cool and trap atoms were available. Molecules offer a number of properties not available in atoms, so experiments with cold trapped molecules promise to generate distinct advances.

Several areas of physics and chemistry can potentially benefit from experiments with cold trapped molecules. Precision spectroscopy may benefit from reduced linewidths and long interaction times of cooled and trapped samples. External-field manipulation, e.g. focusing [5] and guiding, can take advantage of the low translational energy of cooled molecules. Quantum computing with trapped polar molecules has been proposed [6]. Quantum-degenerate gases of molecules are predicted to exhibit novel phenomena, due to strong and anisotropic electric dipole interactions between molecules [7–9]. The sensitivity of certain precision measurements may be increased by the ability to produce large numbers of molecules in a given internal state [10]. The presence of multiple internal degrees of freedom, electric and magnetic dipole moments, reactive channels, and various internal coupling mechanisms make molecular collisions an exciting area [11–13].

All currently-proposed methods for the creation of ultracold molecules (with the exception of photoassociation [14]) rely on the same three stages to achieve ultracold temperatures as experiments with atoms: cooling from room temperature to kelvin-to-mK temperatures, trapping, and further cooling into the ultracold regime. The larger challenge with molecules lies in the first stage of this procedure. Laser cooling, typically used for atoms, is extremely difficult to implement for molecules [15]. An alternative first-stage technique must therefore be used, and several have been developed in the recent years.

Stark deceleration [16] is a general method to slow down polar molecules from a room-temperature supersonic molecular beam; it is applicable to any polar molecule, and was shown to produce up to 10^8 molecules at 30 mK. Velocity selection [17,18], counter-rotating nozzle [19] and billiard-like collisions [20] are also general supersonic beam-based methods, shown to produce small samples of arbitrary molecules at Kelvin-range temperatures.

Buffer gas cooling [21], in which molecules are cooled via elastic collisions with cryogenically cooled helium gas, stands apart from the techniques above in that it is energy-dissipative and therefore more than a slowing method. It accepts the entire Maxwell-Boltzmann distribution of molecules and provides cooling of translational and rotational degrees of freedom in the lab frame. This allows production of cold molecules in numbers far exceeding those demonstrated with any other technique; production of up to 5×10^{13} molecules at 2 K has been demonstrated [22]. The method is completely general and does not rely on the molecule possessing an electric dipole, specific optical transition, or the possibility of high-performance supersonic cooling.

Both photoassociation and the formation of molecules via Feshbach resonances [23] bypass the difficulties of cooling molecules into the ultracold regime by producing them

[a] *Present address*: Department of Molecular Physics, Fritz-Haber-Institut der Max-Planck-Gesellschaft, Berlin, Germany.
[b] e-mail: doyle@physics.harvard.edu

directly from ultracold atoms. Their applicability, however, is limited to molecules made from atoms that can be laser cooled and trapped and has only been demonstrated for alkali dimers.

Buffer gas cooling can produce large numbers of cold molecules. However, in order to achieve this, the molecules themselves have to be generated in large numbers and introduced into the buffer gas on the timescale shorter than the diffusion loss time. Several methods of accomplishing this task have been demonstrated, each of them having its unique strengths.

In laser ablation, an intense laser pulse illuminates a solid precursor target, causing evaporation and fragmentation of the precursor molecules. Laser ablation works quite well for certain molecules, mainly stable diatomics with a solid room-temperature phase (e.g. PbO [10]) and certain radicals (e.g. CaH [24], CaF [22]) with a convenient solid precursor (e.g. CaH_2, CaF_2). An important drawback of the method is the unpredictability of its yield — it is essentially impossible to predict the yield of a given byproduct from a given precursor. Furthermore, for many molecules a convenient solid precursor is not readily available. More importantly, the presence of unwanted ablation byproducts may result in rapid losses of the molecules of interest [25].

Capillary filling is a technique that is well-suited for stable molecules that remain gaseous at low temperatures, e.g. CO [26], NO [27]. A thin capillary connects the low-temperature buffer gas cell with a room-temperature gas supply and molecules are driven into the cell by the supply pressure. The method is simple, but has limited applicability since only stable molecules with high vapor pressures can survive the trip along a thin cold channel without condensing or recombining. The maximum number of molecules that can be loaded using the method is also limited by the requirement that the flux through the capillary be kept low enough to prevent clogging.

In order to circumvent the limitations of laser ablation and capillary filling we have undertaken the development of a novel loading technique — molecular beam loading [28]. With this method, a molecular beam from a room-temperature source is injected into a cryogenic buffer gas cell. This loading technique is very general as decades of molecular beam research have resulted in an ability to produce molecular beams of virtually any species, including unstable molecules. Also, it is possible to remove unwanted byproducts in the beam by introducing standard electrostatic or magnetic filters. In this work, we use the method to produce 10^{12} molecules of NH at <6 K.

Our choice of NH was motivated by a desire to study a Σ-state diatomic molecule with a magnetic moment of $2\mu_B$ since such molecules are expected to be particularly amenable to magnetic trapping in a buffer gas environment [29,30]. Among $^3\Sigma$ molecules, NH also has one of the lowest known ratios of spin-spin to rotation constants, which is predicted to indicate high degree of stability with respect to collision-induced spin depolarization [31]. The NH molecule is polar, with 1.38 Debye dipole moment [32], which makes it particularly interesting for future studies of novel effects in quantum-degenerate gases [7–9] and for possible realization of quantum computing with polar molecules [6]. NH also has four isotopic versions, two bosons and two fermions; in this work we only consider fermionic $^{14}N^1H$, but other isotopic versions can be substituted easily for studies of quantum degeneracy. Finally, NH spectroscopy is well-understood due to its astrophysical importance [33].

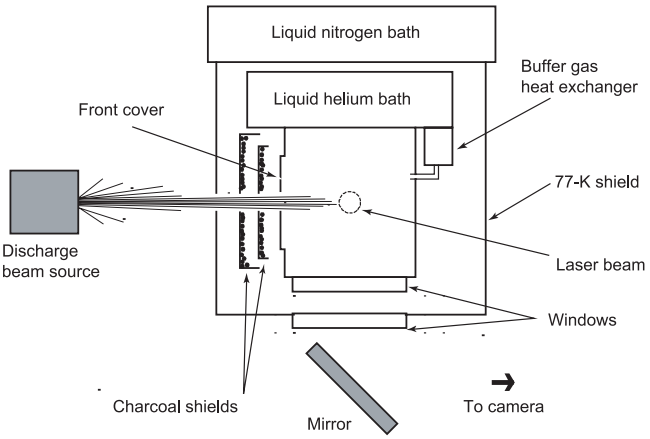

Fig. 1. Schematic of the apparatus. Helium exits the cell through the hole in the front cover (3 mm diameter) while NH from the discharge beam source enters.

2 Experimental details

The apparatus, shown schematically in Figure 1, is similar to the one described in [28]. It consists of a room-temperature radical beam source, a cryogenic buffer gas cell, and a spectroscopic detection system.

The radical beam source is modeled after [34]. It consists of a pulsed solenoid valve (General Valve Series 9) to which an ammonia-based mixture of gases is supplied, and a slit-shaped glow discharge region, which converts ammonia NH_3 molecules in the mixture into NH radicals. The discharge occurs between sharpened metal jaws positioned immediately outside the pulsed valve and held at a negative high voltage, and the metal body of the valve held at ground potential. Electrons and ions from the discharge collide with ammonia molecules and form radicals of interest while other gases in the mixture sustain the discharge by providing avalanche electron multiplication and shield radicals from each other and the walls to prevent recombination. We maximize the production of NH radicals by varying the mixture composition, stagnation pressure, and discharge voltage[1]. Typical parameters used in this

[1] As discharge parameters are varied special care is taken to prevent a transition from glow into arc discharge. The kinetics of an arc discharge are dramatically different from those of glow discharges, and direct comparison between the yields of the two is not possible. An arc discharge has the significant disadvantage of rapid cathode erosion, which introduces an unpredictable time dependence of the discharge parameters.

work are a mixture of 1:9 NH_3:Ar at 2 atm stagnation pressure, −1500 V jaw potential, 1.1 mm inter-jaw separation, 1.52 mm jaw-to-valve separation, 1.6 mm valve nozzle diameter.

The cryogenic part of the apparatus is based on a small liquid helium cryostat with a 1.2 liter helium bath. A cylindrical brass cryocell is thermally anchored to the liquid helium bath. The cryocell is 10 cm long and has an outer diameter of 6 cm and an internal volume of 150 cm^3. The side of the cell facing the molecular beam source has a thin replaceable front cover with a circular orifice 3 mm in diameter through which the molecular beam enters the cell. The cell is filled with helium gas from a room-temperature gas handling system via a 1.1-mm diameter tube. The tube is fitted with a heat exchanger thermally anchored to the helium bath to ensure that incoming helium is at the cell temperature. The gas handling system supplies helium gas at an adjustable steady rate such that the helium pressure in the cell remains constant, balanced by the helium leaving through the cell orifice. The temperature of the cell is monitored by silicon diode thermometers while the pressure inside the cell is monitored by a room-temperature capacitance gauge connected to the cell via a separate 1.9-mm diameter tube.

The liquid helium bath and the cell are surrounded by an aluminum radiation shield connected to a liquid nitrogen bath. Two "charcoal shields" (thin copper cups with 20/40 mesh coconut activated charcoal affixed by epoxy) are placed between the cell orifice and the liquid nitrogen shield to cryopump the helium that leaks out from the cell orifice. The inner charcoal shield is thermally linked to the cell and the outer charcoal shield is thermally linked to the liquid helium bath. Most of the helium atoms leaving the cell are pumped by the inner shield and thus cannot reach the liquid-nitrogen radiation shield. Those that do are likely to hit the outer charcoal shield after they bounce back from the liquid nitrogen shield. The heat imparted to the He atoms by the liquid-nitrogen shield is then deposited in the liquid helium bath and does not increase the temperature of the cryocell.

NH detection and thermalization diagnostics are performed using laser-induced fluorescence and laser absorption spectroscopy on the $A^3\Pi_i(v'=0) \leftrightarrow X^3\Sigma^-(v''=0)$ transition at 336 nm. The molecules are excited with a frequency-doubled cavity-stabilized dye laser on the $R_{31}(0)$: $A^2\Pi_2(v'=0, J'=2) \leftarrow X^3\Sigma^-(v''=0, N''=0, J''=1)$ line at 29770.60 cm^{-1}. Fluorescence from radiative decay on $R_{31}(0)$, $R_{33}(2)$, $Q_{32}(2)$, $P_{31}(2)$, and $P_{33}(4)$ lines is collected with an MCP-intensified CCD camera. The Franck-Condon factor matrix of NH is near-diagonal [35], but since $A^3\Pi_i$ is Hund's case (a) for $J' < 3$ [36], the state leakage is ∼75% per transition [37] and low laser intensities (∼10 $\mu W/mm^2$) must thus be used to avoid spectral hole burning.

The dye laser frequency is controlled with an external voltage source and monitored by a scanning Michelson interferometer (Burleigh WA-1500) and a Fizeau interferometer (Coherent Wavemaster).

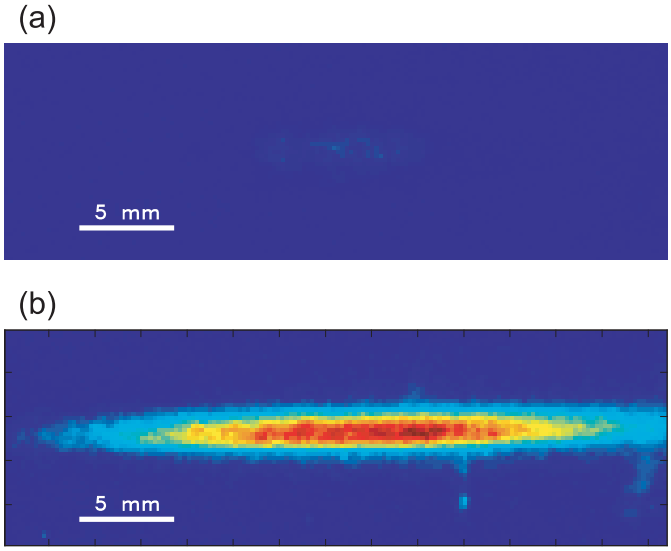

Fig. 2. Typical fluorescence images of NH in cryocell. (a) No buffer gas; some free-flight laser-induced fluorescence seen; (b) buffer gas density 4×10^{16} cm^{-3}; fluorescence distributed along laser beam path. Molecular beam enters the image from the top; probe laser traverses the image left to right. Fluorescence feature dimensions correspond to laser beam width (vertical) and cell size (horizontal). Distance from image center to cell orifice is 32 mm, to valve nozzle –80 mm. A color version of the figure is available at `www.eurphysj.org`.

The camera is fitted with an interference filter that blocks room lights and most of the light from the discharge glow. Since both excitation and fluorescence occur at the same wavelength it is impossible to filter out scattered light from the excitation laser using spectral methods, and technical limitations of the camera readout electronics do not permit temporal filtering. To minimize background light noise, cell windows were fitted with black-oxide coated brass baffles that absorb scattered light. To measure the absolute number of molecules in the cell we calibrate our fluorescence collection using balanced-detector absorption [38].

3 Results

A typical fluorescence image of cold NH radicals in the buffer gas is shown in Figure 2. We observe a weak, localized fluorescence signal for no buffer gas, corresponding to a low-density high-velocity collimated molecular beam, and strong, broad fluorescence for NH accumulating in the buffer gas and diffusing to the walls. The maximum number of NH $X^3\Sigma^-(v''=0, N''=0)$ molecules loaded into the buffer gas cell was measured to be 10^{12}. This number is accurate within an order of magnitude due to uncertainties in the spatial distribution of the molecules in the cell. Large number of NH molecules loaded into the cell suggests that we do not encounter any adverse effects, such as reactive collisions, that may cause radical loss prior to entering the cell.

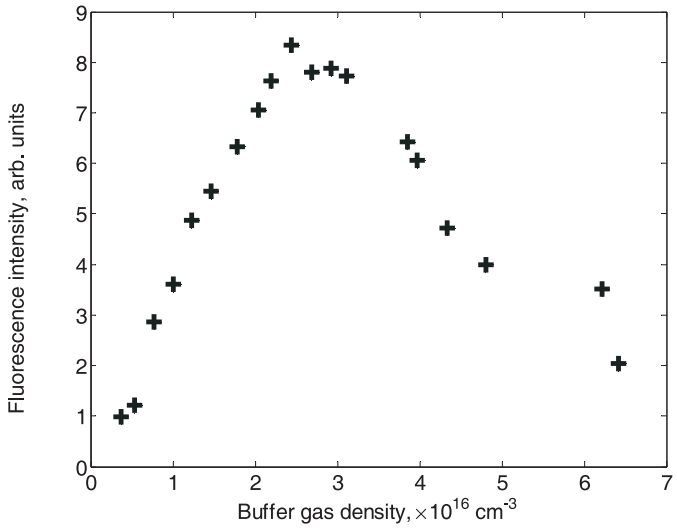

Fig. 3. Effect of buffer gas density on loading efficiency. The efficiency is limited at low densities by lack of NH thermalization and at high density by "crowding" of NH molecules just inside the entrance hole.

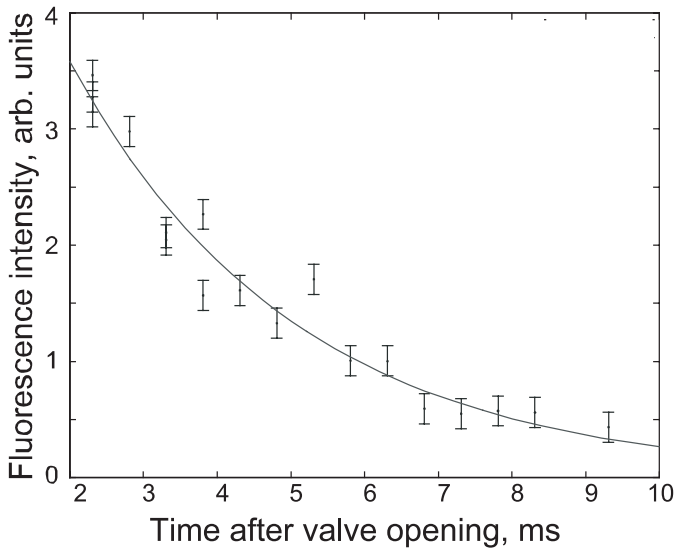

Fig. 4. Fluorescence signal time decay. Loss of molecules is due to diffusion to the cell walls. Markers show integrated fluorescence intensity for $R_{11}(0)$ line on-resonance laser frequency; line is fit to a single exponential. Buffer gas density is 3×10^{16} cm^{-3}.

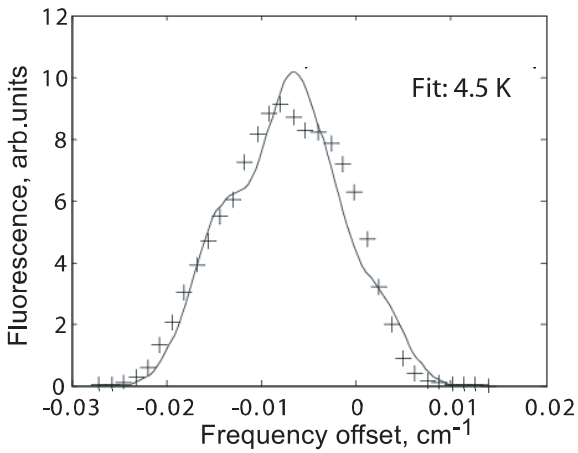

Fig. 5. Translational temperature measurement. Crosses are integrated fluorescence intensity, line is a Voigt profile fit using hyperfine line positions from reference [39].

As expected, the cell loading efficiency exhibits strong dependence on the buffer-gas density. If the density is too low, the molecular beam will not be thermalized. If the density is too high, the molecules will thermalize too close to the cell entrance, and a significant fraction of them will be lost due to wall collisions. In addition, buffer gas emerging from the cell scatters the incoming molecules, introducing a buffer gas density-dependent loss process. The buffer gas pressure in the cell was varied to determine the optimal buffer gas density. The results of this measurement are shown in Figure 3. The peak number is achieved at 3×10^{16} cm^{-3} buffer gas density in the cell, and the loading efficiency decreases away from the peak, as described in [28].

In order to obtain a time-resolved signal profile of NH fluorescence we configured the fluorescence detection camera to acquire data in 500 μs windows with variable time delays. The result of this measurement is shown in Figure 4. The time profile of the signal fits to a single exponential with a time constant of $\tau_{diff} = 3.1 \pm 0.5$ ms, which is consistent with NH diffusing to the walls and getting adsorbed there. This confirms that no unexpected recombination or quenching processes have an effect on the observed NH $X^3\Sigma^-(v'' = 0, N'' = 0)$ population over the timescale of diffusion to the walls. From the fitted value τ_{diff} at a buffer-gas density of 3×10^{16} cm^{-3} we can then extract a lower limit on NH-He elastic cross-section of 1.5×10^{-15} cm^2. The uncertainty comes from lack of precise knowledge of the spatial distribution of molecules. Based on prior experience, we expect the actual value of the cross-section to be within an order-unity factor above the lowerlimit value.

The translational temperature of the molecules was determined by scanning the laser frequency over the $R_{31}(0)$ line and fitting the spectrum to a Doppler-broadened lineshape, as shown in Figure 5. The line profile is composed of twenty-one hyperfine lines spaced over ∼1 GHz [39]. Published measurements of NH hyperfine structure allow us to put an upper limit for translational temperature of $T_{trans} < 6$ K. This limit indicates efficient translational thermalization of NH with the helium buffer gas.

The NH Rotational temperature was determined by comparing the on-resonance fluorescence signal of the $R_{31}(N'' = 0)$ line with that of the $R_{31}(N'' = 1)$ line and assuming a Boltzmann distribution of rotational states. The upper limit for the rotational temperature is $T_{rot} <$ 8 K. As expected, the rotational temperature rapidly comes into equilibrium with the helium buffer gas. The uncertainty in the rotational temperature comes from poor signal-to-noise ratio for measurements on $R_{31}(1)$ line,

the signal for which is over 100 times weaker than that for $R_{31}(0)$.

4 Conclusion

We have confirmed the applicability of beam-loaded buffer gas cooling at 4.2 K to cooling of molecules. We have demonstrated the production of $\sim 10^{12}$ cold molecular radicals and verified their translational (<6 K) and rotational (<8 K) thermalization. The apparatus described can be used to carry out a variety of spectroscopic measurements on atoms, molecules, and metastable species at cryogenic temperatures. With upgrades to the buffer-gas refrigeration mechanism the temperature of the radicals can be lowered to 300 mK without changing the beam or cell geometry. Work is currently underway to trap cold NH radicals from a beam in a superconducting magnetic trap and attempt to evaporatively cool them to ultracold temperatures.

We thank G. Meijer for pointing out the benefits of NH radicals, D. Nesbitt and S. Davis for information on glow discharge source designs, and W. Shoellkopf and B.S. Zhao for assistance with experimental setup. WCC, DE, and SEM acknowledge support from the National Science Foundation Graduate Research Fellowship. This work was supported by the DOE (DE-FG02 ER15316).

References

1. M. Anderson et al., Science **269**, 198 (1995)
2. B.D. Marco, D. Jin, Science **285**, 1703 (1999)
3. R. Onofrio et al., Phys. Rev. Lett. **85**, 2228 (2000)
4. M.O. Mewes et al., Phys. Rev. Lett. **78**, 582 (1997)
5. H. Stapelfeldt et al., Phys. Rev. Lett. **79**, 2787 (1997)
6. D. DeMille, Phys. Rev. Lett. **88**, 067901 (2002)
7. M.A. Baranov et al., Phys. Rev. A **66**, 013606 (2002)
8. L.D. Carr, G.V. Shlyapnikov, Y. Castin, Phys. Rev. Lett. **92** (2004)
9. L. Santos et al., Phys. Rev. Lett. **85**, 1791 (2000)
10. D. Egorov et al., Phys. Rev. A **63**, 030501(R) (2001)
11. N. Balakrishnan, A. Dalgarno, Chem. Phys. Lett. **341**, 652 (2001)
12. J.L. Bohn, Phys. Rev. A **62**, 032701 (2000)
13. R.V. Krems, A. Dalgarno, Phys. Rev. A **67**, 050704 (2003)
14. J. Weiner et al., Rev. Mod. Phys. **71**, 1 (1999)
15. J.T. Bahns, W.C. Stwalley, P.L. Gould, J. Chem. Phys. **104**, 9689 (1996)
16. H.L. Bethlem, G. Berden, G. Meijer, Phys. Rev. Lett. **83**, 1558 (1999)
17. E. Nikitin et al., Phys. Rev. A **68** (2003)
18. S.A. Rangwala et al., Phys. Rev. A **67** (2003)
19. M. Gupta, D. Herschbach, J. Phys. Chem. A **105**, 1626 (2001)
20. M.S. Elioff, J.J. Valentini, D.W. Chandler, Science **302**, 1940 (2003)
21. R. deCarvalho et al., Eur. Phys. J. D **7**, 289 (1999)
22. K. Maussang et al., manuscript in preparation
23. R. Wynar et al., Science **287**, 1016 (2000); M.W. Zwierlein et al., Phys. Rev. Lett. **91**, 250401 (2003)
24. J.D. Weinstein et al., Nature **395**, 148 (1998)
25. J.D. Weinstein et al., J. Chem. Phys. **109**, 2656 (1998)
26. D.R. Willey et al., J. Chem. Phys. **89**, 1923 (1988)
27. D.R. Willey, D.N. Bittner, F.C. Delucia, Mol. Phys. **67**, 455 (1989)
28. D. Egorov et al., Phys. Rev. A **66**, 043401 (2002)
29. J.G.E. Harris et al., Europhys. Lett. **67**, 198 (2004)
30. D. Egorov, *Buffer-Gas Cooling of Diatomic Molecules* (Harvard University, 2004)
31. R.V. Krems et al., Phys. Rev. A **68**, 051401 (2003)
32. E.A. Scarl, F.W. Dalby, Can. J. Phys. **52**, 1429 (1974)
33. T. Klaus, S. Takano, G. Winnewisser, Astron. Astrophys. **322**, L1 (1997)
34. S. Davis et al., J. Chem. Phys. **107**, 5661 (1997)
35. S.N. Suchard, J.E. Melzer, *Spectroscopic data* (IFI/Plenum, New York, 1975)
36. R.N. Dixon, Can. J. Phys. **37**, 1171 (1959)
37. A. Schadee, Astron. Astrophys. **41**, 213 (1975)
38. R. Claps et al., Appl. Opt. **40**, 4387 (2001)
39. W. Ubachs, J.J. Ter Meulen, A. Dymanus, Can. J. Phys. **62**, 1374 (1984)